Chinese Chemical Letters 34 (2023) 107665

Contents lists available at ScienceDirect

Chinese Chemical Letters

journal homepage: www.elsevier.com/locate/cclet

Lighting up rotaxanes with AIEgens

Xiao-Qin Xu[a], Xu-Qing Wang[a], Wei Wang[a,b,*]

[a] School of Chemistry and Molecular Engineering, East China Normal University, Shanghai 200062, China
[b] Guangdong Provincial Key Laboratory of Functional and Intelligent Hybrid Materials and Devices, South China University of Technology, Guangzhou 510640, China

ARTICLE INFO

Article history:
Received 26 April 2022
Revised 23 June 2022
Accepted 5 July 2022
Available online 10 July 2022

Keywords:
Mechanically interlocked molecules
Aggregation-induced emission
Molecular shuttles
Förster resonance energy transfer
Light harvesting
Aggregate

ABSTRACT

Aiming at the construction of novel rotaxanes with desired luminescent properties for practical applications, recently the rapid development of rotaxanes decorated with aggregation-induced emission (AIE) luminogens (*i.e.,* AIEgens) has been witnessed. The combination of AIEgens and rotaxanes leads to the successful construction of a novel type of luminescent rotaxanes with many attractive features. In particular, the unique controllable dynamic feature of rotaxanes endows the resultant AIEgen-based rotaxanes precisely tunable emissions under external stimuli, leading to the construction of a novel type of smart luminescent materials. In this minireview, the recent progress of AIEgen-based rotaxanes has been summarized, with an emphasis on the design strategy and potential applications.

1. Introduction

As a fundamental and typical class of mechanically interlocked molecules (MIMs) [1–8], a rotaxane [9–16] is composed of two parts: wheel components and dumbbell-like axle components, which are holding together by mechanical bonds (Fig. 1a). Attributed to their unique interlocked structures as well as the controllable nanoscale motion behaviors, rotaxanes have proven to be privileged platforms for the construction of artificial molecular machines [17–21]. For instance, when the axle component of a rotaxane contains multiple stations with different binding affinities with its wheel component, the wheel component can move along the axle under specific external stimuli, thus leading to a molecular shuttle [22–26]. Notably, in 2016, two pioneers in rotaxane-based molecular machines, *i.e.,* Sauvage [27] and Stoddart [28], were awarded the Nobel Prize in Chemistry jointly with B.L. Feringa, opening up a new gold era of research in rotaxanes and other MIMs. During the past few decades, in addition to the construction of novel molecular machines such as molecular muscles, molecular assemblers, molecular pumps, molecular cable cars [29–34], rotaxanes have been also widely applied in diverse fields such as sensing, drug delivery, and catalysis, making them promising platforms for practical applications [35,36].

In particular, aiming at the construction of novel rotaxanes with intriguing photophysical properties, the rapid development of luminescent rotaxanes has been witnessed [37]. By attaching selected fluorophores to the rotaxane skeletons, a series of functional rotaxanes with tunable emissive features have been successfully constructed, which have showed great potential for wide applications such as sensing, bioimaging, and information storage [38–41]. However, most traditional fluorophores would suffer from typical aggregation-induced quenching (ACQ) effect in the aggregate state, thus might hamper the further explorations of the applications of corresponding luminescent rotaxanes [42,43]. To deal with such key issue, Tang *et al.* developed a novel class of luminogens (*i.e.,* AIEgens) with attractive aggregation-induced emission (AIE) features, which are typically non-emission in solution but intensively emissive in the aggregate state attributed to the restriction of intramolecular rotation (RIR) [44–46]. During past two decades, the research in AIE has evolved to the birth of aggregology [47]. Many typical AIEgens such as tetraphenylethene (TPE), hexaphenylsilole (HPS), and 9,10-distyrylanthracene (DSA) have been developed, which have been widely used in bioimaging, sensors, optoelectronic devices and many other fields [48,49].

The combination of AIEgens and rotaxanes would give rise to a novel type of luminescent rotaxanes with many attractive features (Figs. 1b and c). First of all, it would further expand the applications of luminescent rotaxanes from solution state to aggregate state, thus offering great opportunities for the developing novel luminescent materials. In addition, the formation of interlocked structures in rotaxanes could influence the AIE behaviors

* Corresponding author at: School of Chemistry and Molecular Engineering, East China Normal University, Shanghai 200062, China.
E-mail address: wwang@chem.ecnu.edu.cn (W. Wang).

https://doi.org/10.1016/j.cclet.2022.07.008
1001-8417/

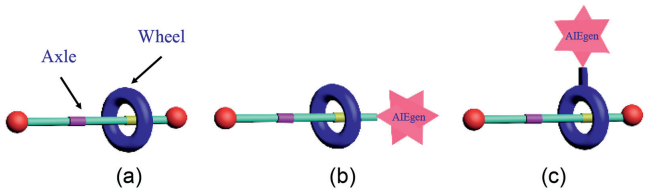

Fig. 1. (a) Cartoon illustrations of [2]rotaxane, (b) [2]rotaxane with AIEgen on the axle component, (c) [2]rotaxane with AIEgen on the wheel component.

of AIEgens through mechanical bonds, which might efficiently enhance their AIE effect [50]. Notably, for some rotaxanes, it might be also AIE-active even without traditional AIEgens in their structures [51]. More importantly, taking advantage of the unique dynamic feature of rotaxanes would lead to the construction of novel smart luminescent materials with precisely tunable emissions, thus further expanding their application scope. Attributed to these attractive features, recently AIEgen-based rotaxanes have attracted more and more attention and some significant progress has been made. In this minireview, the recent progress of AIEgen-based rotaxanes has been summarized, with an emphasis on the design strategy and potential applications.

2. Rotaxanes with AIEgens on the axle components

In 2015, Yin and coworkers demonstrated the first report on the construction of AIEgen-based rotaxanes [52]. In their study, tetraphenylethene (TPE), the most typical AIEgen, was selected as the stoppers for the synthesis of a series of rotaxanes, including [2]rotaxanes **2** and **6** as well as [3]rotaxanes **4** (Fig. 2). Starting from axle components containing both TPE and dialkylammonium moieties, these rotaxanes were prepared through a template-directed clipping approach [53]. By using acetonitrile as a good solvent and water as a poor solvent, the AIE behaviors of these resultant rotaxanes and corresponding axle components was then evaluated. For [2]rotaxanes **2a** and **2b**, comparing with the axle **1**, more obvious AIE effect was observed according to the photoluminescence (PL) spectra since the dramatic enhancement in luminescence for these systems was observed upon increasing the water fraction (f_w) to 85% for **1**, 80% for **2a**, and 70% for **2b**, respectively (Fig. 3a). In addition, according to such result, [2]rotaxane **2b** with a long alkyl chain revealed better aggregation then that of **2a**. Such phenomenon was possibly attributed to the larger overlap between the host macrocycle in **2b** than that of **2a**, which has been supported by the theoretical DFT calculation. In the case of [3]rotaxanes **4a** and **4b**, similar trend in their AIE behaviors as that of the [2]rotaxanes was observed (Fig. 3b). According to these results, the introduction of the wheel components in rotaxanes was proven to promote the formation of aggregate state. Moreover, the existence of long alkoxyl chains would further enhance such process. To confirm such effect, new axle **5** as well as [2]rotaxanes **6a** and **6b** with longer distance between the TPE and ammonium units were further designed and synthesized. Interestingly, in this new system, due to the long distance between the macrocycle and the TPE units, there was no obvious overlap between them that led to the weakening of the restricted intramolecular rotation (RIR) process of the TPE unit, thus their AIE behaviors were similar (Fig. 3c). According to this study, the formation of rotaxanes, especially ones with functional groups, did influence the AIE behaviors, which offers good opportunities for the constructions of novel rotaxanes with tunable AIE emissions.

In the same year, on the basis of previous work described above, the same group further synthesized another AIE-active [2]rotaxane **7a** with TPE as a stopper [54]. Notably, in [2]rotaxane **7a**, both the ammonium and amide moieties were introduced as recognition sites, and at the same time *N*-hetero crown ether ring was introduced as the wheel component. In their design strategy,

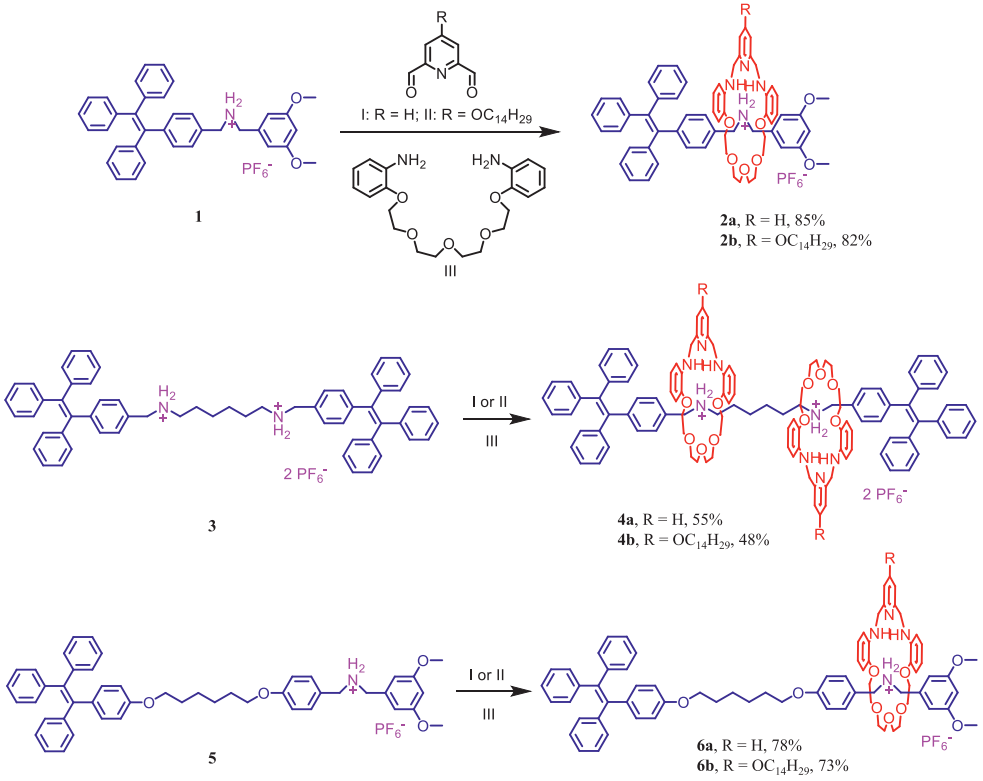

Fig. 2. Synthesis of [2]rotaxanes **2a**-**2b**, **6a**-**6b** and [3]rotaxanes **4a**–**4b**.

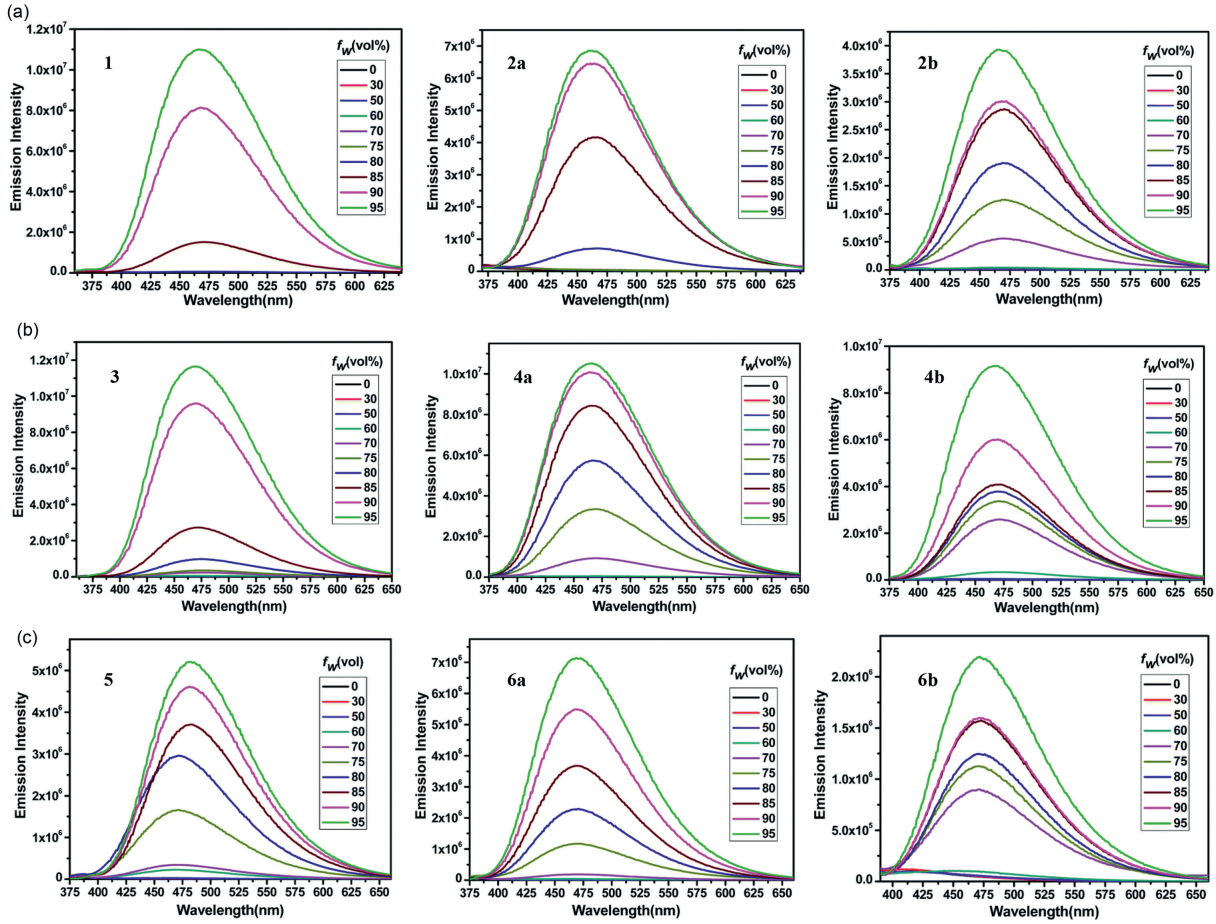

Fig. 3. (a) fluorescence spectra of **1** (left), **2a** (middle), and **2b** (right) in CH_3CN-water mixtures with different water fractions. (b) fluorescence spectra of **3** (left), **4a** (middle), and **4b** (right) in CH_3CN-water mixtures with different water fractions. (c) fluorescence spectra of **5** (left), **6a** (middle), and **6b** (right) in CH_3CN-water mixtures with different water fractions. Copied with permission [52]. Copyright 2015, Royal Society of Chemistry.

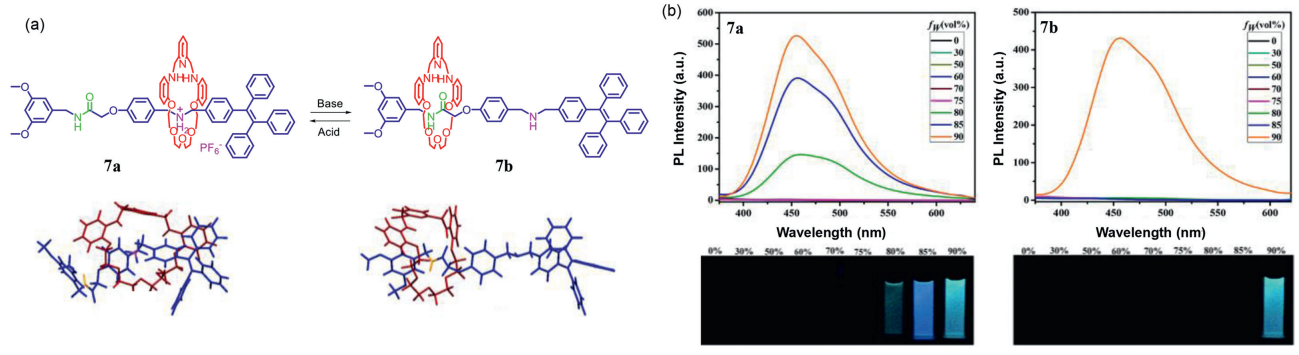

Fig. 4. (a) Chemical and energy-minimized structures of [2]rotaxnes **7a** and **7b** whose wheel component could be relocated on the axle component though the deprotonation and re-protonation. (b) Fluorescence spectra and photographs of **7a** (left) and **7b** (right) in CH_3CN-water mixtures with different water fractions ($\lambda_{ex} = 340$ nm). Reproduced with permission [54]. Copyright 2015, Royal Society of Chemistry.

by using acid and base as external stimulus, the controllable shuttling motion of the wheel component between the ammonium station and the amide station would be realized, which might lead to the modulation of the AIE behaviors of the resultant molecular shuttle (Fig. 4a). To confirm such hypothesis, the AIE behaviors of the rotaxane in both protonated and deprotonated states were investigated (Fig. 4b). It was found that for protonated rotaxane **7a**, upon increasing the water fraction (f_W) to 80%, the fluorescence of **7a** increased rapidly. However, for the deprotonated rotaxane **7b**, no fluorescence was observed until the f_W reached 90%. Such phenomenon might be attributed to that in **7b** the wheel component was located at the amide recognition site, which was far from the TPE unit, thus the interaction is weakened, which leads to a reduction in the degree of TPE rotation restriction. It is proved that in rotaxane-based molecular shuttles the interaction between the wheel component and AIEgens could be readily adjusted by external stimuli, which further tuned the aggregation states of AIEgen-based rotaxanes, thereby leading to switchable optical outputs.

Considering the emerging wide biomedical applications of fluorescent probes with AIE characteristics, in 2016, Huang and coworkers demonstrated the successful construction of a novel platform based on AIEgen-based rotaxane as targeting, imaging

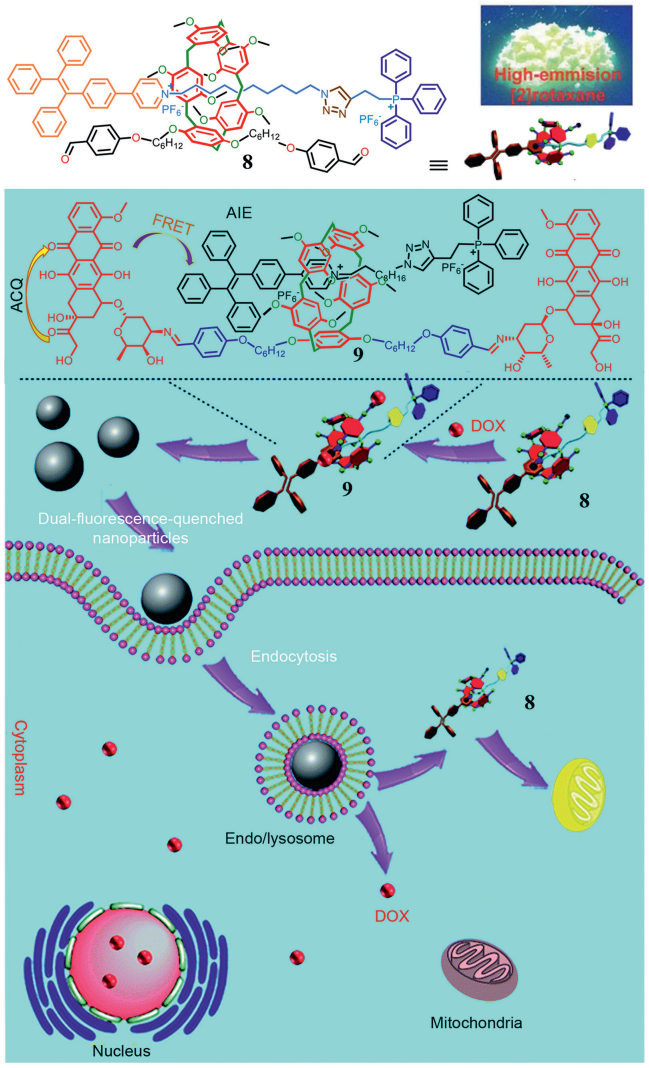

Fig. 5. Chemical structure of high-emission [2]rotaxane **8** (top) and schematic illustration of the preparation of the mitochondria-targeting probe-inspired prodrug [2]rotaxane **9** and possible cellular pathways of the dual-fluorescence-quenched **9** nanoparticles (bottom).

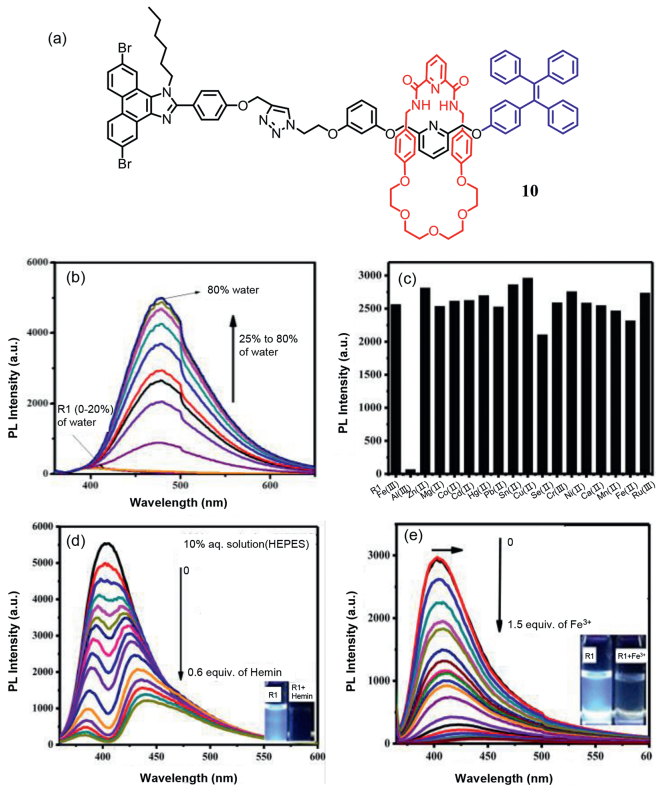

Fig. 6. (a) Chemical structure of [2]rotaxane **10**. (b) Fluorescence spectra of **10** with increasing water fraction (from 25% to 80%). (c) Bar diagram depicting fluorescence quenching of **10** in 10% aq., HEPES (pH 7.4, 10 mmol/L) in DMSO with various metal ions. (d) Fluorescence spectra of **10** in 10% aq., HEPES (pH 7.4, 10 mmol/L) in DMSO with increasing concentration of Fe^{3+} metal ion. (e) Fluorescence titration spectra of **10** in the presence of Hemin in 10% aq., HEPES (pH 7.4, 10 mmol/L) in DMSO. Reproduced with permission [66]. Copyright 2016, Elsevier Ltd.

and therapeutic agents [55]. In their study, TPE and triphenylphosphonium (TPP) groups was introduced as stoppers, which acted as an AIE-active fluorogen and mitochondria-targeting site, respectively (Fig. 5). In addition, pillar[5]arene (P[5]A) macrocycles functionalized with two aldehyde units was selected as the wheel component [56–65]. The targeted [2]rotaxane **8** was synthesized through a one-pot copper(I)-catalyzed azide-alkyne cycloaddition (CuAAC) reaction. Notably, similar with previous report, the formation of [2]rotaxane significantly enhanced the AIE effect of [2]rotaxane **8** comparing with the corresponding free axle due to the RIR process of TPE unit. Impressively, on the basis of the attractive emission feature of **8**, nanoparticles (NPs) self-assembled from it was further prepared a reprecipitation technique, which displayed high specificity to mitochondria and superior photostability. Furthermore, attributed to the existence of aldehyde moieties in the wheel component of [2]rotaxane **8**, anticancer drugs containing amine groups such as doxorubicin (DOX) could be further introduced into the rotaxane through the formation of imine bonds, resulting in **9** as a novel drug delivery platform. Notably, due to the Förster resonance energy transfer (FRET) process between TPE and DOX units, the introduction of DOX quenched the fluorescence of **9**. Further hydrolysis of the imine bonds in the in the cell led to not only the release of DOX but also the recovery of the fluorescence since the FRET process between these two fluorophores were no longer existed, making such system quite attractive for bioimaging applications.

Through the conventional metal template approach, Lin and coworkers reported the synthesis of [2]rotaxane **10** with TPE and phenanthroimidazole (PIZ) unit as the stoppers (Fig. 6a) [66]. In this study, the DMSO/water solvent system was employed for the investigation of the AIE behavior of **10**. It was found that when the water fraction (f_w) was 10%, the PIZ unit contributed to the fluorescence emission at 401 nm. When f_w was above 20% and up to 80%, remarkable AIE effect with bright blue at 470 nm was observed attributed to the aggregation process (Fig. 6b). Moreover, the existence of hetero-atoms "N" and "O" within the unique interlocked structure of [2]rotaxane was further employed for sensing applications. Interestingly, in both the non-aggregated ($f_w = 10\%$) and aggregated states ($f_w = 80\%$) of **10**, among many tested alkali and transition metal ions, the addition of Fe^{3+} led to a significant fluorescence quenching (Figs. 6c and d). Further fluorescence quenching experiments also indicated the sensing capability of **10** for Hemin, a real small biomolecule containing Fe^{3+}, even with a higher sensitivity (Fig. 6e).

Very recently, by using double TPE units as stoppers and the dibenzo-24-crown-8 (DB24C8) macrocycle as wheel component, the same group demonstrated the construction of a series of AIE-active [2]rotaxanes **11–13** (Fig. 7a) [67]. In addition to the investigations on the formation of various nanostructures upon aggregation, these resultant [2]rotaxanes were also used for ion recognition, but for anions. As shown in Fig. 7, AIE tests indicated

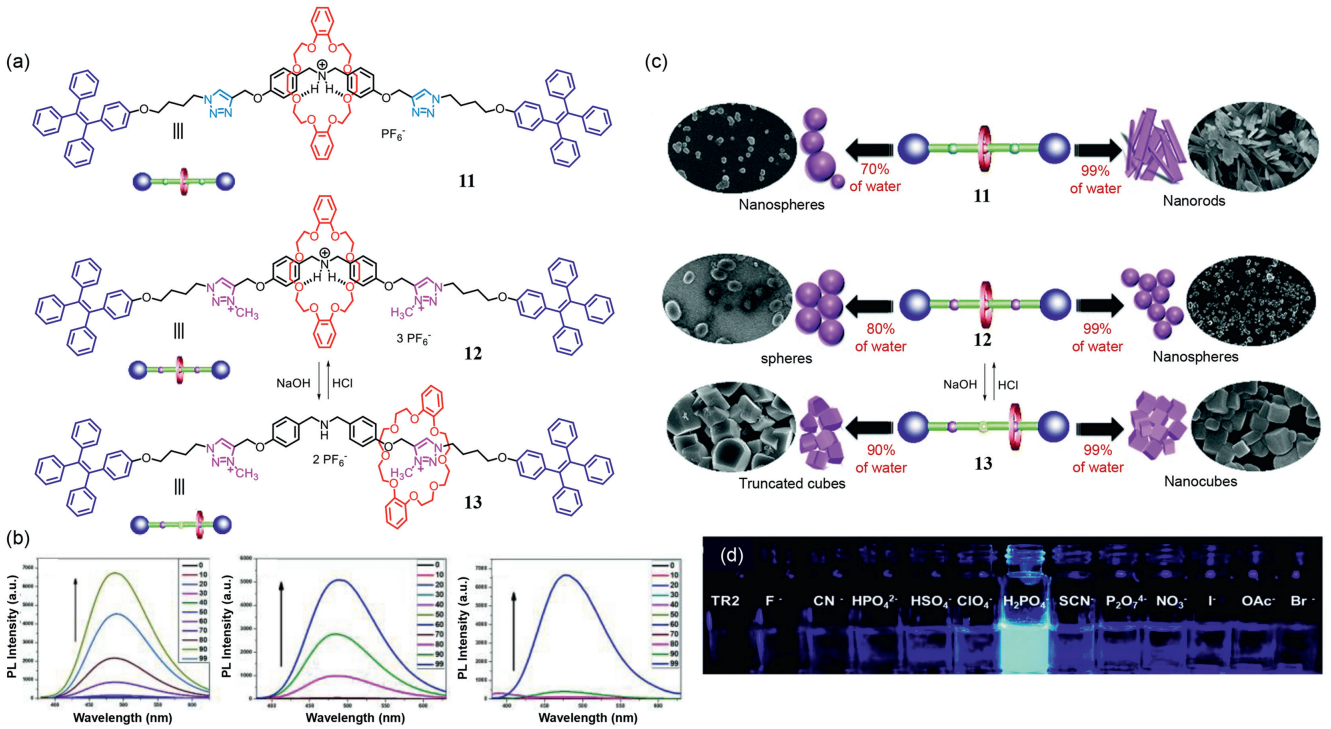

Fig. 7. (a) Chemical structures of [2]rotaxanes **11–13**. (b) Fluorescence spectra of [2]rotaxanes **11** (left), **12** (middle), and **13** (right) (10 mmol/L) in CH_3CN/water solutions with different water fractions. (c) Schematic representations of diverse self-assembled nanostructures of [2]rotaxanes **11–13** in CH_3CN/water solutions at different water fractions. (d) Fluorescence color changes in the presence of various TBA salts in CH_3CN solutions of [2]rotaxane **12**. Reproduced with permission [67]. Copyright 2021, Royal Society of Chemistry.

that depending on their structures, different [2]rotaxanes started to show AIE behaviors at varied the water fraction (f_w) values (70% for **11**, 80% for **12**, and 90% for **13**) (Fig. 7b). Many key factors such as molecular shuttling of the wheel component and the interactions between the wheel component and TPE units as well as the viscosities of the solvents used for AIE tests was proven to influence their AIE behaviors.

Interestingly, upon the aggregation process, for different [2]rotaxanes, varied self-assembled nanostructural morphologies were observed. For instance, when **11** was dissolved in pure acetonitrile, nanospheres with an average diameter of 200 nm were formed. When $f_w = 70\%$, the size of the nanospheres decreased to around 150 nm. When $f_w = 90\%$, nanorods were formed due to the fusion of nanoaggregates. In the case of **12**, when dissolved in pure acetonitrile, spheres with a size of 2.0 μm were formed. And when f_w was increased to 80%, nanospheres were formed. For **13**, the initial morphology in pure acetonitrile was nanospheres with an average size of 250 nm. When $f_w = 90\%$, a truncated cubic structure with a size of 2.0 μm was found, and the further increase of f_w to 99% resulted in the formation of nanocubic structure (Fig. 7c). Moreover, attributed to the existence of 1,2,3-triazolium rings that could interact with anion species through hydrogen bonding or dipole-dipole interactions, the investigations on the anion sensing ability of [2]rotaxane **12** were further performed. The results indicated that **12** revealed a turn-on response towards dihydrogen phosphate ($H_2PO_4^-$) with a binding constant of 7.72×10^3 L/mol calculated by the fluorescence titration profile as well as 1:1 binding stoichiometry determined by Job's plots (Fig. 7d).

Actually, in 2017, Cao and coworkers have already demonstrated the synthesis of AIE-active [2]rotaxane with double TPE units as stoppers [68]. In their study, cucurbit[10]uril (CB[10]) with large cavity was employed as wheel component. On the basis of the host-guest interaction between CB[10] and viologen moiety, the targeted [2]rotaxane was successfully synthesized in 81% yield

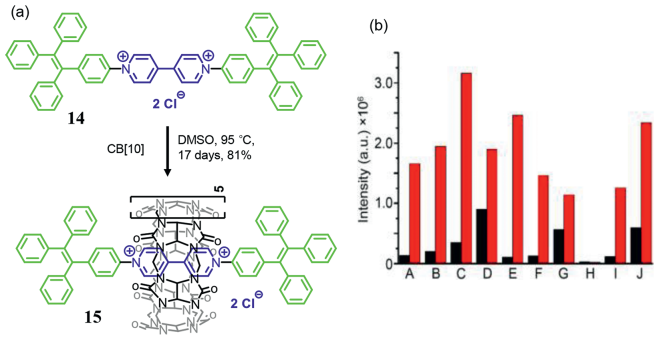

Fig. 8. (a) Synthesis of [2]rotaxane **15** from the axle component **14** through the slipping method. (b) Fluorescence intensity at 600 nm of **14** (10 μmol/L, black column) and **15** (10 μmol/L, red column) in different solvents including 1% DMSO (A = acetone; B = CH_2Cl_2; C = $CHCl_3$; D = 1,4-dioxane; E = DMF; F = DMSO; G = EA; H = H_2O; I = MeOH; J = THF). λ_{ex} = 365 nm; Ex/Em slits = 5/5 nm. Copied with permission [68]. Copyright 2017, American Chemical Society.

through the slipping method by heating the axle component **14** with two TPE units and CB[10] in DMSO at 95 °C for 17 days (Fig. 8a). Notably, for the axle component **14**, it was nonfluorescent in DMSO. Upon the formation of corresponding [2]rotaxane **15**, the RIR process of the TPE stoppers made **15** highly fluorescent in DMSO with the quantum yield up to 0.50. Moreover, when studying the influence of solvent on the AIE behavior of **15**, it was found that no matter in which solvent, the fluorescence intensity of [2]rotaxane **15** was always stronger than that of the axle component **14**, highlighting the enhanced AIE effect through the formation of [2]rotaxane (Fig. 8b). In particular, upon further addition of chloroform and tetrahydrofuran into the DMSO solution of [2]rotaxane **15**, further increase in the fluorescence intensity was observed, indicating an interesting stepwise aggregation-induced emission enhancement.

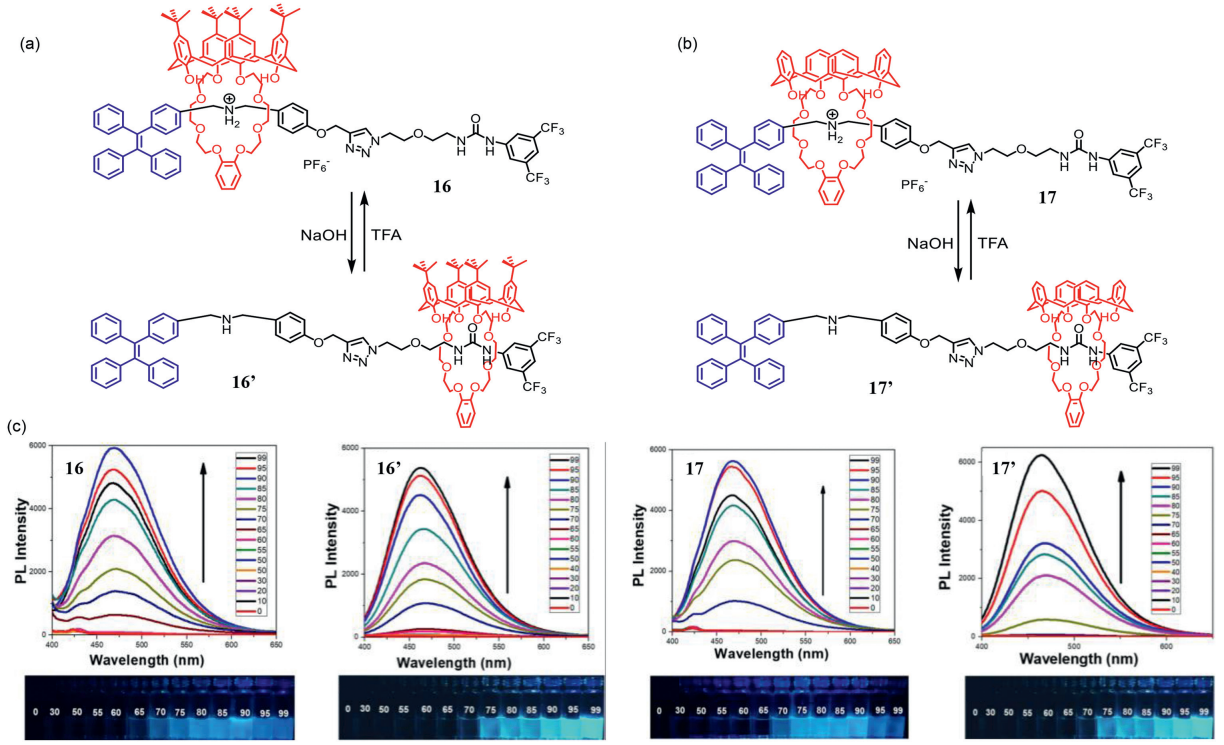

Fig. 9. (a) Chemical structures of acid/base switchable [2]rotaxanes **16** and **16′**. (b) Chemical structures of acid/base switchable [2]rotaxanes **17** and **17′**. (c) Fluorescence spectra and emission photographs of [2]rotaxanes **16**, **16′**, **17**, and **17′** in CH_3CN/water cosolvent system with different water fractions. Reproduced with permission [69]. Copyright 2018, American Chemical Society.

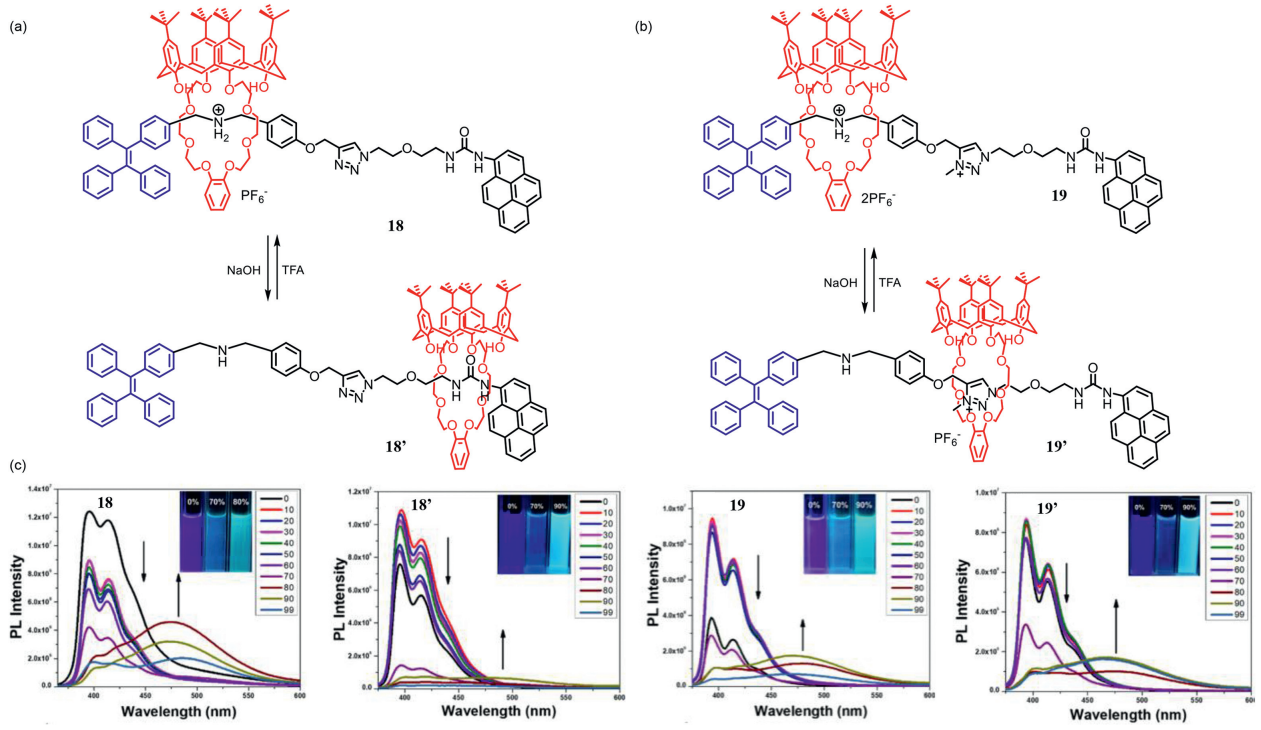

Fig. 10. (a) Chemical structures of acid/base switchable [2]rotaxanes **18** and **18′**. (b) Chemical structures of acid/base switchable [2]rotaxanes **19** and **19′**. (c) Fluorescence spectra and emission photographs of [2]rotaxanes **18**, **18′**, **19** and **19′** in THF/water cosolvent system with different water fractions. Reproduced with permission [70]. Copyright 2018, American Chemical Society.

Aiming at the construction of switchable supramolecular amphiphiles based on AIE-active [2]rotaxanes, in 2018, Chung and coworkers demonstrated the synthesis of [2]rotaxanes **16** and **17**, both of which were decorated with TPE unit as the capping group and calix[4]arene either with or without *t*–butyl as the wheel components, respectively [69]. For these [2]rotaxanes, due to the existence of both ammonium and urea moieties as two stations in the axle, the reversible switching between them with the wheel component locating at the ammonium station and corresponding deprotonated [2]rotaxanes **16′** and **17′** with the wheel components staying at the urea station was successfully achieved by using acid/base stimuli (Figs. 9a and b). These four [2]rotaxanes

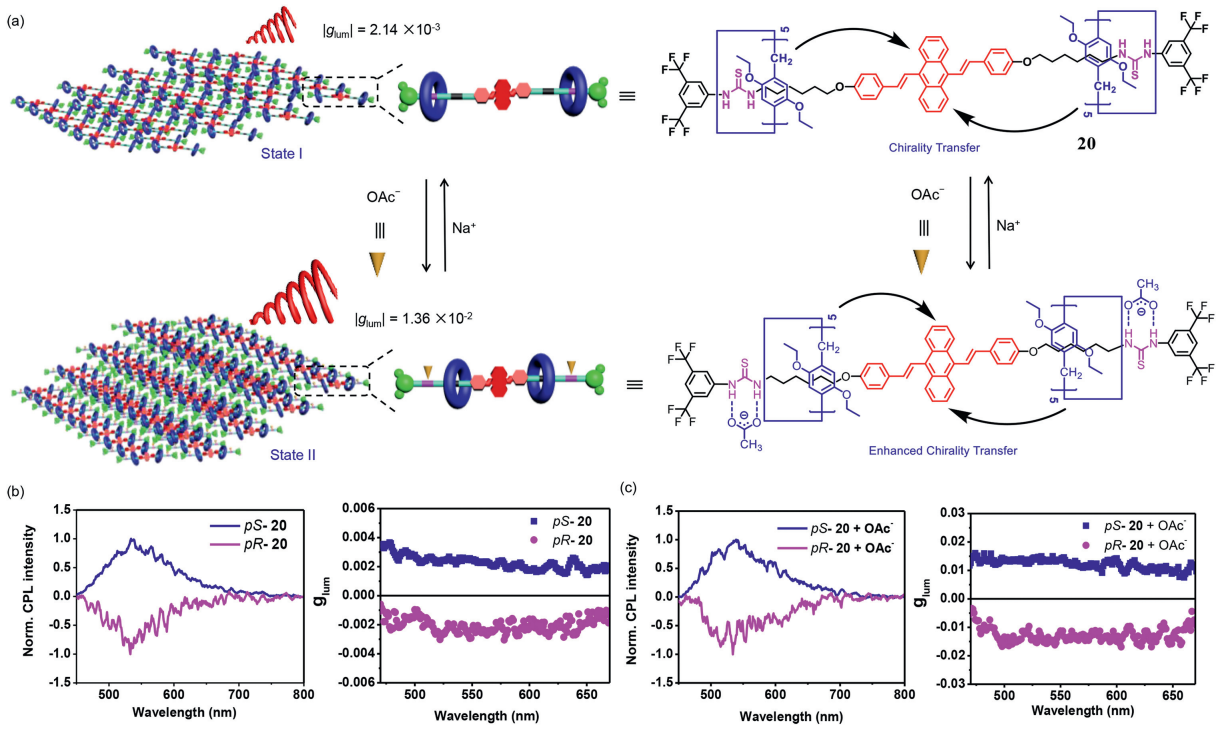

Fig. 11. (a) Design strategy of novel CPL switching system based on the AIE-active chiral [3]rotaxane **20** upon the addition or removal of acetate anions as external stimuli. (b) CPL spectra (left) and g_{lum} spectra (right) of the cast film of *pS*-**20** and *pR*-**20**. (c) CPL spectra (left) and g_{lum} spectra (right) of the cast film of *pS*-**20** and *pR*-**20** upon the addition of acetate anions. Reproduced with permission [71]. Copyright 2021, Wiley-VCH GmbH.

exhibited different AIE effects and unique characteristics of nanostructures under different water contents. For **16** and **16′**, upon the gradual increase of water fractions in CH_3CN, they started to aggregate and emit when $f_w = 65\%$ and 70%, respectively, and for **17** and **17′** such values were $f_w = 70\%$ and 75% respectively (Fig. 9c). For **16**, because TPE is closer to the macrocycle, the effect is stronger, and there are multiple interactions such as urea-based intermolecular hydrogen bonding, van der Waals force between tert–butyl groups, which makes it have AIE at relatively low water content effect.

Further research on its nanostructure found that when the protonated rotaxanes **16** and **17** are in a pure acetonitrile solution, a microsphere structure will be formed; when the f_w is 65% and 70%, respectively, nanospheres will be formed; when the water content is further increased at 90%, nanospheres with reduced size will be formed. For the rotaxanes **16′** and **17′** in the deprotonated state, when f_w is 70% and 75%, hollow nanospheres will be formed; when $f_w = 99\%$, a nanosphere structure will be formed. It proves that the structural transformation can be driven by different f_w values and molecular shuttles. It is worth mentioning that due to the existence of multiple interactions, **16** can form a gel state in methanol solution. When the concentration is low, it will form a spherical structure. When the concentration is high, it will form a dumbbell-

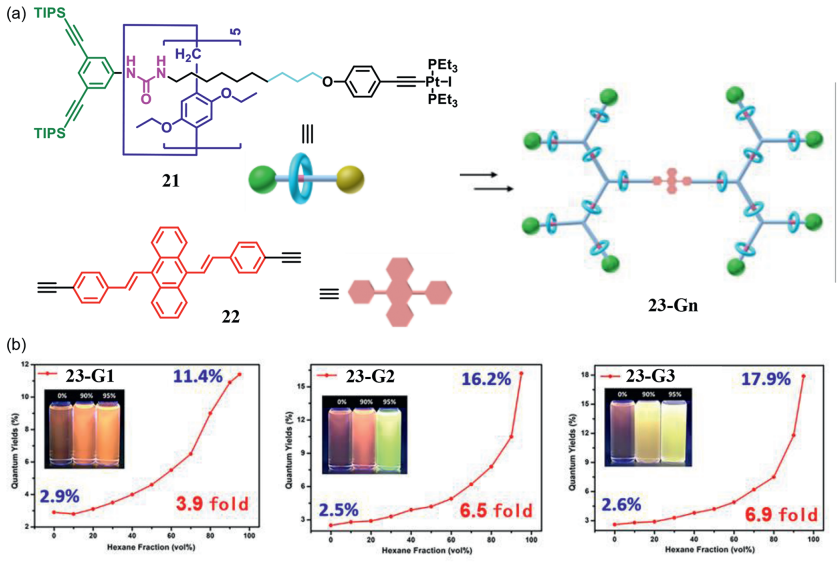

Fig. 12. (a) Synthesis of the AIE-active rotaxane dendrimers **23-Gn** through the controllable divergent approach from [2]rotaxane **21** and DSA precursor **22** as key building blocks. (b) Fluorescence quantum yields of **23-G1** (left), **23-G2** (middle), and **23-G3** (right) in CH_2Cl_2/*n*-hexane with various *n*-hexane fractions. Reproduced with permission [76]. Copyright 2019, Royal Society of Chemistry.

shaped 3D cross-linked network structure. The reversible transformation of sol-gel can be realized under the control of acid and alkali.

In 2020, by further introducing pyrene unit as the other stopper, the same group demonstrated the synthesis of [2]rotaxanes **18** and **19** with both AIE and ACQ fluorophores on their axle components [70]. Similar with previous report, these resultant [2]rotaxanes were also switchable upon the reversible base/acid treatment, resulting in the corresponding [2]rotaxane **18′** and **19′**, respectively (Figs. 10a and b). For all [2]rotaxanes, only the emission bands at 395 and 415 nm attributed to the pyrene monomer were observed in pure THF. Upon the addition of water as poor solvent to trigger the aggregation, a new emission band appeared at 485 nm when $f_w = 70\%$, indicating that the AIE effect of TPE unit (Fig. 10c). For **18**, when further increasing the f_w to 80%, the AIE effect reached the maximum along with a remarkable blue shift. While for other three [2]rotaxanes, supreme bright fluorescence enhancement was achieved when f_w reached 90%. Due to the formation of nanoaggregates that suppressed the emissive decay pathways, the further increment of water fraction to 99% only led to fainted fluorescence enhancement.

In addition to [2]rotaxanes as described above, the AIEgen could also be introduced into [3]rotaxanes. For instance, in 2021, Wang, He and coworkers demonstrated the preparation of novel AIEgen-based [3]rotaxane **20**, from which switchable circularly polarized luminescence (CPL) system was successfully constructed (Figs. 11a) [71]. In their study, another typical AIEgen DSA unit was introduced as the center of axle component in [3]rotaxane **20**. In addition, two pillar[5]arene macrocycles (DEP[5]A) was introduced as the wheel components. Due to the existence of urea moiety as stimuli-responsive sites in the axle component, [3]rotaxane **20** revealed unique stimuli-responsiveness towards acetate anions. Upon the addition or removal of acetate anions, controllable motions of DEP[5]A wheels along the axle was realized. AIE tests indicated that [3]rotaxane displayed typical AIE behaviors with the fluorescence quantum yield of $(25.8 \pm 1.2)\%$ in aggregate state.

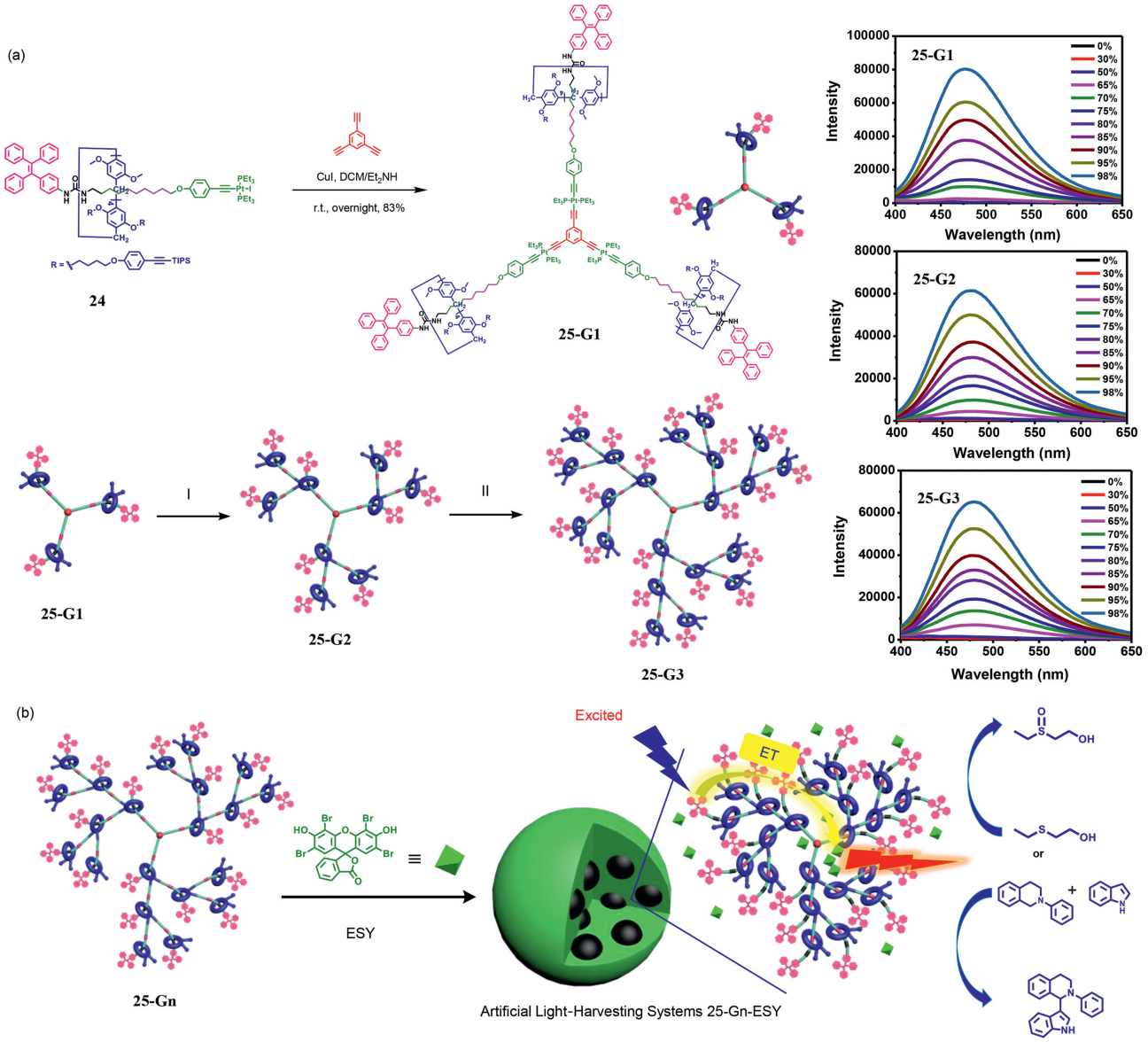

Fig. 13. (a) Synthesis of the AIEgen-branched rotaxane dendrimers **25-Gn** through the controllable divergent approach from [2]rotaxane **24** (left) and fluorescence spectra of in CH_2Cl_2/MeOH with various MeOH fractions (right). Reaction conditions: (I): (a) $Bu_4NF{\cdot}3H_2O$, THF, r.t., 2 h; (b) **24**, CuI, DCM/Et_2NH, r.t., overnight, 70%; (II): (a) $Bu_4NF{\cdot}3H_2O$, THF, r.t., 2 h; (b) **24**, CuI, DCM/Et_2NH, r.t., overnight, 38%. (b) The construction of artificial LHSs based on TPE-branched rotaxane dendrimers **25-Gn** and ESY as efficient photocatalysts. Reproduced with permission [81]. Copyright 2021, Wiley-VCH GmbH.

In addition, the switching process triggered by acetate anion led to a slight decrease of fluorescence quantum yield to (24.3 ± 2.6)%. More importantly, owing to the conformation-dependent planar chirality of DEP[5]A wheels, three stereoisomer of [3]rotaxane **20**, *i.e.*, a pair of enantiomers and a mesomer, were separated by chiral preparative HPLC. For the resultant chiral [3]rotaxanes, along with the switching process, the relocation of chiral DEP[5]A wheels resulted in expected enhanced chirality information transfer, as revealed by CD spectra. Impressively, upon the addition of acetate anions, CPL tests indicated a 6.4-fold enhancement in high dissymmetry factors (g_{lum}) from $\pm$ 2.14 × 10^{-3} to $\pm$ 1.36 × 10^{-2} (Figs. 11b and c). Notably, such CPL switching process revealed excellent cycling ability, making it quite attractive for practical applications.

Aiming at the construction of novel mechanically bonded macromolecules with intriguing photophysical properties, AIEgens have been also introduced into rotaxane dendrimers [72–75]. In an earlier report in 2019, Yang and coworkers demonstrated the construction of novel AIE-active rotaxane-branched dendrimers with DSA unit as the core (Fig. 12a) [76]. Starting from a DSA precursor **22** with two alkyne units, the employment of a neutral organometallic [2]rotaxane **21** as key building block led to the successful synthesis of rotaxane-branched dendrimers **23-Gn** (n = 1, 2, 3) through a controllable divergent approach with up to 14 individual [2]rotaxanes as branches. AIE tests indicated that, for all the resultant rotaxane-branched dendrimers, they displayed typical AIE behaviors upon the gradual addition of *n*-hexane as a poor solvent. Notably, attributed to the varied steric hindrances originated from the surrounding rotaxane branches, these rotaxane-branched dendrimers revealed interesting generation-dependent AIE behaviors. For instance, in the non-aggregate state, the fluorescence quantum yields of all the rotaxane-branched dendrimers were almost the same (for **23-G1**, 2.9%; for **23-G2**, 2.5%; for **23-G3**, 2.6%). While in the aggregate state, more remarkable enhancements in fluorescence quantum yields were observed for higher-generation rotaxane-branched dendrimers (for **23-G1**, 11.4%, 3.9-fold; for **23-G2**. 16.2%, 6.5-fold; for **23-G3**, 17.9%, 6.9-fold) (Fig. 12b). Such phenomenon indicated that the increase of dendrimer generation led to more obvious AIE effect, thus providing a new approach for the construction of novel luminescent functional materials with tunable AIE behaviors.

Recently, based on their on-going interest in function-oriented rotaxane dendrimers, the same group further reported the construction of novel AIEgen-branched rotaxane dendrimers [77–80], based on which artificial light harvesting systems (LHSs) were further prepared [81]. In this study, TPE unit was introduced into as a stopper [2]rotaxane **24**, from which rotaxane dendrimers **25-Gn** (n = 1, 2, 3) up to the third generation were synthesized through the same controllable divergent approach (Fig. 13a). In the resultant rotaxane dendrimers, AIEgens were precisely-arranged at each branch, making them the first successful example of AIEgen-branched rotaxane dendrimers. Interestingly, attributed to the existence of urea moiety at the axle of each rotaxane branches, the resultant rotaxane dendrimers revealed a two-step aggregation behavior depending on the fraction of MeOH that was added as not only poor solvent to drive the aggregation but also external stimuli to interact with the urea moieties. Low fraction of MeOH triggered the contraction of rotaxane dendrimers through the MeOH-induced switching translational motions of the pillar[5]arene wheels located at both the branches and branching points. By increasing the MeOH fractions, the further aggregation of the resultant contracted rotaxane dendrimers took place, simultaneously leading to the remarkable enhancement in the emission intensity.

Furthermore, by choosing eosin Y (ESY) as the fluorescence energy acceptor, corresponding artificial LHSs were then constructed, which was clearly revealed by the fluorescence spectra. Interestingly, along with the increase of the generation of rotaxane dendrimers, enhancements in both energy-transfer efficiencies (for **25-G1**-ESY, 42.5%; for **25-G2**-ESY, 68.2%; for **25-G3**-ESY, 71.6%) and antenna effect (for **25-G1**-ESY, 1.1; for **25-G2**-ESY, 2.3; for **25-G3**-ESY, 4.1) of the resultant artificial LHSs was observed, revealing an interesting generation-dependent effect. Impressively, these artificial LHSs were proven to act as efficient photocatalysts for both photooxidation reaction and aerobic cross-dehydrogenative coupling (CDC) reaction (Fig. 13b), and their photocatalytic performances were also generation-dependent. According to this study, the integration of multiple AIEgen-based rotaxanes in well-defined arrangements would serve as promising platform for the construction of novel functional supramolecular materials for practical applications.

In a very recent report, in addition to TPE-based [2]rotaxane **24**, another [2]rotaxane **26** decorated with two anthracene units was employed by the same group as functionalized building blocks as well as tetraethynylpyrene unit **27** as both core module and energy acceptor (Fig. 14a), leading to the successful construction of novel rotaxane dendrimers **28-Gn** (n = 1, 2, 3) with both AIE and

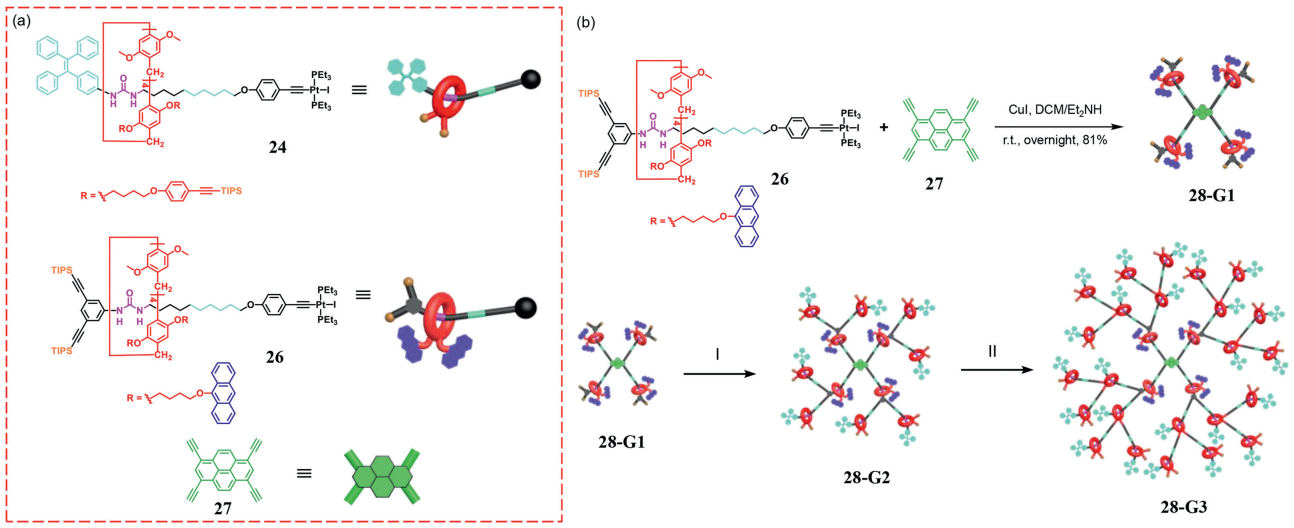

Fig. 14. Chemical structures of the key building blocks (a) for the synthesis of rotaxane dendrimers **28-Gn** as novel LHSs through the controllable divergent approach (b). Reaction conditions: (I): (a) $Bu_4NF{\cdot}3H_2O$, THF, r.t., 2 h, 87%; (b) **24**, CuI, DCM/Et_2NH, r.t., overnight, 70%; II): (a) $Bu_4NF{\cdot}3H_2O$, THF, r.t., 2 h, 70%; (b) **24**, CuI, DCM/Et_2NH, r.t., overnight, 71%. Reproduced with permission [82]. Copyright 2022, Elsevier Ltd.

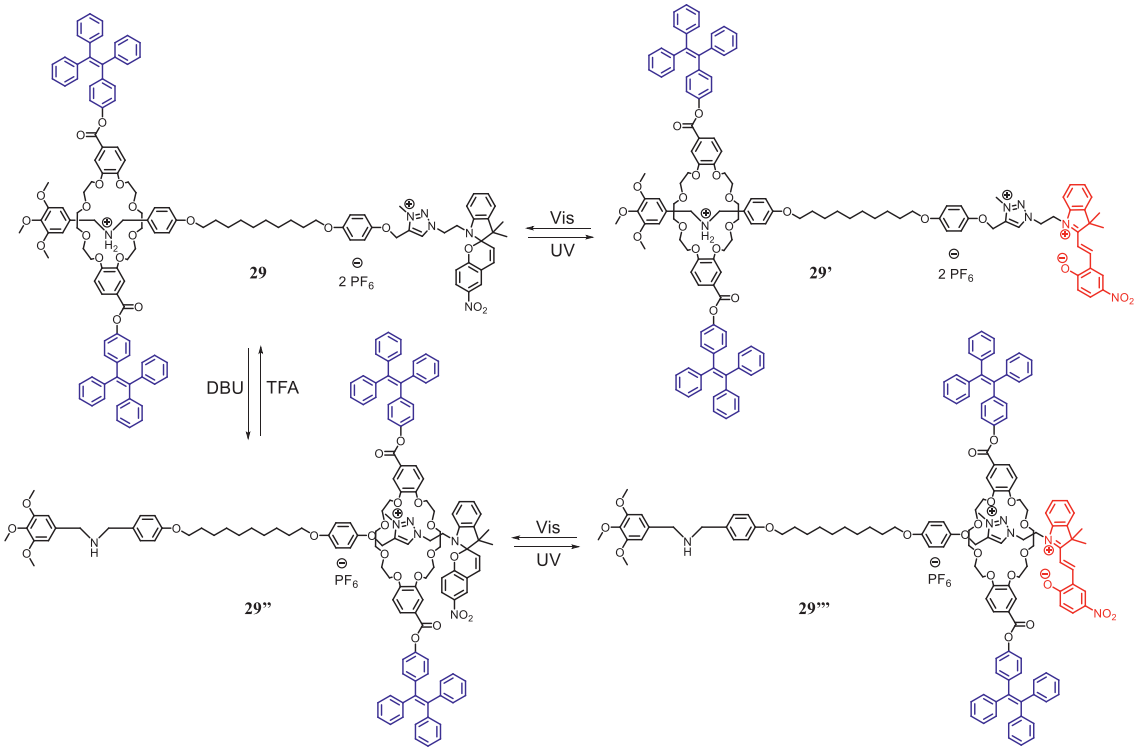

Fig. 15. Reversible transformations between [2]rotaxanes **29**, **29′**, **29′′**, and **29′′′**.

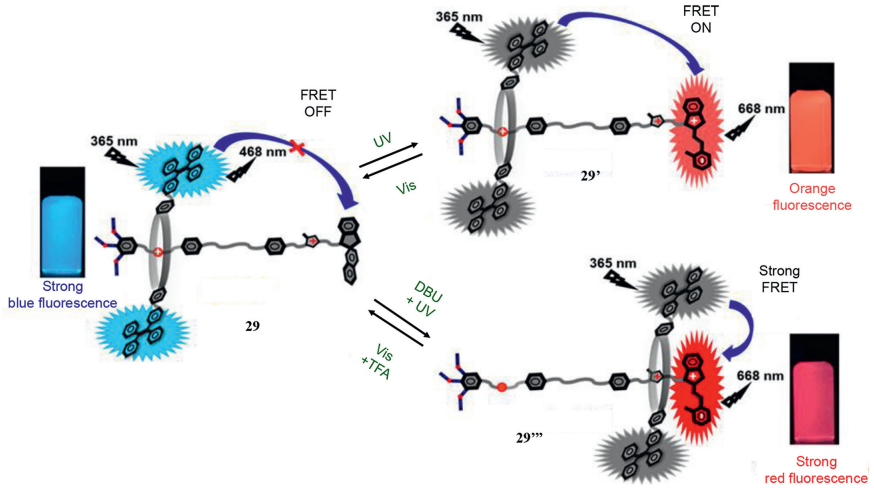

Fig. 16. Tunable emission behaviors of these [2]rotaxanes in different states. Reproduced with permission [83]. Copyright 2020, American Chemical Society.

ACQ luminogens as energy donors through the controllable divergent approach (Fig. 14b) [82]. Similar with the AIEgen-branched rotaxane dendrimers **25-Gn** described above, the resultant rotaxane dendrimers, including two hetero ones, also revealed solvent-induced switching feature, making them excellent platforms for the construction of artificial LHSs with tunable light harvesting ability. Interestingly, similar generation-dependent effect was observed through the fluorescence spectra, enhanced antenna effects were observed along with the increase of dendrimer generation, thus providing another promising candidate as efficient photocatalysts.

3. Rotaxanes with AIEgens on the wheel components

In addition to the introduction of AIEgens into the axle components of rotaxanes mainly as stoppers, it can be also attached on the wheel component. For instance, in 2020, Lin and coworkers reported a novel photo-switchable [2]rotaxane **29** with spiropyran (SP) unit, a classical photochromic moiety, as a stopper [83]. In [2]rotaxane **29**, crown ether ring modified with two TPE units was selected as the wheel component. In addition, due to the insertion of both the secondary ammonium and *N*-methyltriazolium units in the axle component, the wheel component could undergo reversible shuttling between these two stations through the deprotonation/protonation process by adding base or acid. Together with the photo-induced transformation between the closed form SP and the open form MC, the reversible transformations between **29**, **29′**, **29′′**, and **29′′′** were successfully realized (Fig. 15).

More importantly, attributed to the FRET process between the TPE units in the wheel component and MC stopper as well as the acid-base induced distance changes between them, the emission behaviors of these [2]rotaxanes in different states could be pre-

cisely adjusted (Fig. 16). For instance, in the initial state, due to the absence of FRET between the TPE and SP moiety, [2]rotaxane **29** emitted strong blue fluorescence in the aggregate state. Up UV irradiation that induced the formation of MC unit, the FRET between TPE and MC unit resulted in an orange fluorescence emission of [2]rotaxane **29′**. Moreover, by deprotonation of the secondary ammonium using DBU to trigger the movement of the wheel component to the *N*-methyltriazolium station, the reduced distance between TPE and MC units led to enhanced FRET, thus making [2]rotaxane **29′′′** reveal a strong red fluorescence. This report provides a nice example of the precise regulation of emission behaviors of AIEgen-based [2]rotaxanes based on their unique dynamic feature.

4. Conclusion

During past few years, through the introduction of typical AIEgens into either the axle or wheel components, the successful construction of diverse AIEgen-based rotaxanes have been achieved. The formation of rotaxanes through mechanical bonds did significantly influence the AIE effect, thus leading to a novel type of luminescent materials. More importantly, by using the concept of molecular shuttles, rotaxanes with tunable AIE behaviors have been also constructed, whose emission properties could be well regulated through external stimuli-induced re-locations of AIEgens within rotaxane skeleton. Attributed to these attractive structural and emissive features, AIEgen-based rotaxanes have been applied in diverse fields such as sensing, bioimaging, CPL switching, and light harvesting.

Although some impressive progress has been made, the research in AIEgen-based rotaxanes is still in an early stage, more efforts are still greatly needed. For instance, the further construction of AIEgen-based rotaxanes with sufficient diversity in both structures and properties is still necessary. According to the in-depth investigations of these diverse rotaxanes, the structure-property relationship of AIEgen-based rotaxanes would be established, which could promote the further function-oriented design of new AIE-active rotaxanes with desired properties and functions. Moreover, in addition to the combination of dynamic feature of rotaxanes with AIEgens toward the construction of smart luminescent materials, the integration of the chiral rotaxanes, particularly the mechanically planar chiral ones [84,85], with AIEgens would lead to AIEgen-based rotaxanes with switchable chiroptical properties, which would serve as excellent candidates for the construction of novel chiral materials.

Declaration of competing interest

The authors declare that they have no known competing financial interests or personal relationships that could have appeared to influence the work reported in this paper.

Acknowledgments

We acknowledge the financial support sponsored by the National Natural Science Foundation of China (No. 22001073), the Fundamental Research Funds for the Central Universities and the Research Fund Program of Guangdong Provincial Key Laboratory of Functional and Intelligent Hybrid Materials and Devices (No. 2020-GDKLFSHMD-07).

References

[1] J.F. Stoddart, Chem. Soc. Rev. 38 (2009) 1802–1820.
[2] R.S. Forgan, J.P. Sauvage, J.F. Stoddart, Chem. Rev. 111 (2011) 5434–5464.
[3] E.A. Neal, S.M. Goldup, Chem. Commun. 50 (2014) 5128–5142.
[4] C.J. Bruns, J.F. Stoddart, The Nature of the Mechanical Bond: From Molecules to Machines, John Wiley and Sons, Hoboken, 2016.
[5] J.E.M. Lewis, M. Galli, S.M. Goldup, Chem. Commun. 53 (2017) 298–312.
[6] M. Denis, S.M. Goldup, Nat. Rev. Chem. 1 (2017) 0061.
[7] H.Y. Zhou, Y. Han, C.F. Chen, Mater. Chem. Front. 4 (2020) 12–28.
[8] D. Sluysmans, J.F. Stoddart, Trends Chem. 1 (2019) 185–197.
[9] J.P. Sauvage, Eur. J. Org. Chem. (2019) 3287–3288.
[10] Q. Shi, C.F. Chen, Chem. Sci. 10 (2019) 2529–2533.
[11] X. Fu, Q. Zhang, S.J. Rao, et al., Chem. Sci. 7 (2016) 1696–1701.
[12] S.J. Rao, Q. Zhang, J. Mei, et al., Chem. Sci. 8 (2017) 6777–6783.
[13] R. Liu, Y. Zhang, W. Wu, et al., Chin. Chem. Lett. 30 (2019) 577–581.
[14] X.Q. Wang, W.J. Li, W. Wang, et al., Chem. Commun. 54 (2018) 13303–13318.
[15] G.Y. Wu, X. Shi, H. Phan, et al., Nat. Commun. 11 (2020) 3178.
[16] W. Wang, B. Sun, X.Q. Wang, et al., Chem. Eur. J. 21 (2015) 6286–6294.
[17] S. Erbas-Cakmak, D.A. Leigh, C.T. McTernan, et al., Chem. Rev. 115 (2015) 10081–10206.
[18] L. Zhang, V. Marcos, D.A. Leigh, Proc. Natl. Acad. Sci. U. S. A. 115 (2018) 9397–9404.
[19] Q. Wang, D. Chen, H. Tian, Sci. China Chem. 61 (2018) 1261–1273.
[20] A.W. Heard, S.M. Goldup, ACS Cent. Sci. 6 (2020) 117–128.
[21] W. Wang, H.B. Yang, Sci. Bull. 65 (2020) 1964–1965.
[22] P.L. Anelli, N. Spencer, J.F. Stoddart, J. Am. Chem. Soc. 113 (1991) 5131–5133.
[23] R.A. Bissell, E. Córdova, A.E. Kaifer, et al., Nature 369 (1994) 133–137.
[24] S. Chen, Y. Wang, T. Nie, et al., J. Am. Chem. Soc. 140 (2018) 17992–17998.
[25] K. Zhu, C. O'Keefe, V.N. Vukotic, et al., Nat. Chem. 7 (2015) 514–519.
[26] K. Zhu, G. Baggi, S.J. Loeb, Nat. Chem. 10 (2018) 625–630.
[27] J.P. Sauvage, Angew. Chem. Int. Ed. 56 (2017) 11080–11093.
[28] J.F. Stoddart, Angew. Chem. Int. Ed. 56 (2017) 11094–11125.
[29] B. Lewandowski, G. De Bo, J.W. Ward, et al., Science 339 (2013) 189–193.
[30] C. Cheng, P.R. McGonigal, S.T. Schneebeli, et al., Nat. Nanotechnol. 10 (2015) 547–553.
[31] M.C. Jiménez, C. Dietrich-Buchecker, J.P. Sauvage, Angew. Chem. Int. Ed. 39 (2000) 3284–3287.
[32] Y. Qiu, L. Zhang, C. Pezzato, et al., J. Am. Chem. Soc. 141 (2019) 17472–17476.
[33] Z. Meng, C.F. Chen, Chem. Commun. 51 (2015) 8241–8244.
[34] Z. Meng, J.F. Xiang, C.F. Chen, Chem. Sci. 5 (2014) 1520–1525.
[35] M. Xue, Y. Yang, X. Chi, et al., Chem. Rev. 115 (2015) 7398–7501.
[36] H.Y. Zhou, Q.S. Zong, Y. Han, et al., Chem. Commun. 56 (2020) 9916–9936.
[37] X. Ma, H. Tian, Chem. Soc. Rev. 39 (2010) 70–80.
[38] M. Denis, J. Pancholi, K. Jobe, et al., Angew. Chem. Int. Ed. 57 (2018) 5310–5314.
[39] X. Ma, J. Zhang, J. Cao, et al., Chem. Sci. 7 (2016) 4582–4588.
[40] W. Liu, A. Johnson, B.D. Smith, J. Am. Chem. Soc. 140 (2018) 3361–3370.
[41] E. Arunkumar, C.C. Forbes, B.C. Noll, et al., J. Am. Chem. Soc. 127 (2005) 3288–3289.
[42] J. Luo, Z. Xie, J.W.Y. Lam, et al., Chem. Commun. (2001) 1740–1741.
[43] B.Z. Tang, X. Zhan, G. Yu, et al., J. Mater. Chem. 11 (2001) 2974–2978.
[44] J. Mei, N.L.C. Leung, R.T.K. Kwok, et al., Chem. Rev. 115 (2015) 11718–11940.
[45] B. Jiang, C.W. Zhang, X.L. Shi, et al., Chin. J. Polym. Sci. 37 (2019) 372–382.
[46] L.J. Chen, Y.Y. Ren, N.W. Wu, et al., J. Am. Chem. Soc. 137 (2015) 11725–11735.
[47] B.Z. Tang, Aggregate 1 (2020) 4–5.
[48] B. Liu, B.Z. Tang, Angew. Chem. Int. Ed. 59 (2020) 9788–9789.
[49] Z. Zhao, H. Zhang, J.W.Y. Lam, et al., Angew. Chem. Int. Ed. 59 (2020) 9888–9907.
[50] H.V. Miyagishi, H. Masai, J. Terao, Chem. Eur. J. 28 (2021) e202103175.
[51] X. Hou, C. Ke, C.J. Bruns, et al., Nat. Commun. 6 (2015) 6884.
[52] G. Liu, D. Wu, J. Liang, et al., Org. Biomol. Chem. 13 (2015) 4090–4100.
[53] P.T. Glink, A.I. Oliva, J.F. Stoddart, et al., Angew. Chem. Int. Ed. 40 (2001) 1870–1875.
[54] X. Han, M. Cao, Z. Xu, et al., Org. Biomol. Chem. 13 (2015) 9767–9774.
[55] G. Yu, D. Wu, Y. Li, et al., Chem. Sci. 7 (2016) 3017–3024.
[56] T. Ogoshi, T. Aoki, R. Shiga, et al., J. Am. Chem. Soc. 134 (2012) 20322–20325.
[57] L.L. Zhao, Y. Han, C.G. Yan, Chin. Chem. Lett. 31 (2020) 81–83.
[58] C. Ke, N.L. Strutt, H. Li, et al., J. Am. Chem. Soc. 135 (2013) 17019–17030.
[59] Y. Han, C.Y. Nie, S. Jiang, et al., Chin. Chem. Lett. 31 (2020) 725–728.
[60] N.L. Strutt, R.S. Forgan, J.M. Spruell, et al., J. Am. Chem. Soc. 133 (2011) 5668–5671.
[61] J. Ye, R. Zhang, W. Yang, et al., Chin. Chem. Lett. 31 (2020) 1550–1553.
[62] K. Yang, S. Chao, F. Zhang, et al., Chem. Commun. 55 (2019) 13198–13210.
[63] M. He, L. Chen, B. Jiang, et al., Chin. Chem. Lett. 30 (2019) 131–134.
[64] Y. Hu, W. Wang, R. Yao, et al., Mater. Chem. Front. 3 (2019) 2397–2402.
[65] H. Chong, C. Nie, L. Wang, et al., Chin. Chem. Lett. 32 (2021) 57–61.
[66] T. Shukla, A.K. Dwivedi, R. Arumugaperumal, et al., Dyes Pigment. 131 (2016) 49–59.
[67] R. Arumugaperumal, M. Shellaiah, Y.K. Lai, et al., J. Mater. Chem. C 9 (2021) 3215–3228.
[68] Y. Yu, Y. Li, X. Wang, et al., J. Org. Chem. 82 (2017) 5590–5596.
[69] R. Arumugaperumal, P. Raghunath, M.C. Lin, et al., Chem. Mater. 30 (2018) 7221–7233.
[70] R. Arumugaperumal, M. Shellaiah, V. Srinivasadesikan, et al., ACS Appl. Mater. Interfaces 12 (2020) 45222–45234.
[71] W.J. Li, Q. Gu, X.Q. Wang, et al., Angew. Chem. Int. Ed. 60 (2021) 9507–9515.
[72] X.Q. Wang, W.J. Li, W. Wang, et al., Acc. Chem. Res. 54 (2021) 4091–4106.
[73] W. Wang, L.J. Chen, X.Q. Wang, et al., Proc. Natl. Acad. Sci. U. S. A. 112 (2015) 5597–5601.
[74] X.Q. Wang, W. Wang, W.J. Li, et al., Nat. Commun. 9 (2018) 3190.
[75] X.Q. Wang, W.J. Li, W. Wang, et al., J. Am. Chem. Soc. 141 (2019) 13923–13930.
[76] X.Q. Wang, W. Wang, W.J. Li, et al., Org. Chem. Front. 6 (2019) 1686–1691.
[77] W.J. Li, Z. Hu, L. Xu, et al., J. Am. Chem. Soc. 142 (2020) 16748–16756.

[78] W.J. Li, X.Q. Wang, W. Wang, et al., Giant 2 (2020) 100020.
[79] Z. Peng, X.Q. Xu, X.Q. Wang, et al., Chem. Commun. 58 (2022) 2006–2009.
[80] W.J. Li, W. Wang, X.Q. Wang, et al., J. Am. Chem. Soc. 142 (2020) 8473–8482.
[81] W.J. Li, X.Q. Wang, D.Y. Zhang, et al., Angew. Chem. Int. Ed. 60 (2021) 18761–18768.
[82] W.J. Li, H. Jiang, X.Q. Wang, et al., Mater. Today Chem. 24 (2022) 100874.
[83] P.Q. Nhien, T.T.K. Cuc, T.M. Khang, et al., ACS Appl. Mater. Interfaces 12 (2020) 47921–47938.
[84] E.M.G. Jamieson, F. Modicom, S.M. Goldup, Chem. Soc. Rev. 47 (2018) 5266–5311.
[85] N.H. Evans, Chem. Eur. J. 24 (2018) 3101–3112.